Proceedings of the 10th World Congress on Mechanical, Chemical, and Material Engineering (MCM'24)
Barcelona, Spain –August 22-24, 2024
Paper No. HTFF 279
DOI: 10.11159/htff24.279

Optimization of an Autonomous Underwater Vehicle Using a Gradient-Based Approach

Roham Lavimi[1], Alla Eddine Benchikh Lehocine[1], Sébastien Poncet [1], Bernard Marcos[2], Raymond Panneton[1]
[1]Centre de Recherche Acoustique-Signal-Humain (CRASH), Département de génie mécanique, Université de Sherbrooke
2500 bd de l'Université, Sherbrooke (QC), J1K 2R1, Canada
Roham.Lavimi@Usherbrooke.ca
[2]Département de génie chimique et de génie biotechnologique, Université de Sherbrooke
2500 bd de l'Université, Sherbrooke (QC), J1K 2R1, Canada

Abstract **-** In this research, an adjoint method is employed to optimize the nose and tail of an Autonomous Underwater Vehicle (AUV). The drag force, which has a significant impact on energy consumption, is considered as an objective function to be minimized, while the partial volume is chosen as a constraint. The entire procedure is carried out utilizing two open-source softwares: Salome (CAD and mesh generator) and OpenFOAM v2206 (CFD solver and optimizer). Reynolds-averaged Navier-Stokes equations with the k-ω SST turbulence model are used to simulate the turbulent flow around the AUV. Besides, the constrained optimization is performed using the adjointOptimisationFoam, a 3D steady-state adjoint Navier-Stokes incompressible solver in OpenFOAM v2206. The drag force obtained from this study is validated against experimental results, indicating a good agreement (a 0.58% discrepancy). According to the results, the optimized AUV indicates a 3.25% reduction in drag force over the baseline after nine optimization cycles.

Keywords**:** AUV Optimization, Gradient-Based Method, Adjoint Method, Drag Force

1. Introduction

The use of Autonomous Underwater Vehicles (AUVs) is becoming more prevalent in scientific and commercial fields due to their advantages of versatility and low cost compared to manned vehicles [1, 2]. AUV is one of the most cutting-edge technologies developed in global maritime engineering over the last two decades, combining a variety of technologies, including energy, sensing, navigation, communication, and propulsion technologies [2].

A majority of AUVs have a relatively short range because of energy technology restrictions, making them incapable of performing operations on a broad scale of time and space [3]. AUVs are typically powered by either lithium-ion batteries [4] or fuel cells [5]. One way to address the challenge of long-term maritime operations by AUVs is to minimize their power requirements [6]. As a substantial percentage of power loss is attributable to the resistance provided by the water to the AUV, an in-depth study of the hydrodynamic characteristics can result in the fabrication of AUVs with optimum shape control and navigation systems [7]. Various studies have been theoretically [8], experimentally [9], and numerically [10] carried out to investigate the hydrodynamic characteristics of AUVs. Computational Fluid Dynamics (CFD) has been widely employed as a potent analysis tool for predicting the hydrodynamic forces and flow characteristics of AUVs due to its cheap computing cost, high efficiency, and good accuracy [11]. Several numerical studies have been carried out to predict the hydrodynamic forces of AUVs. For example, Dantas and De Barros [10] numerically investigated the effects of control surface deflection and the angle of attack on the hydrodynamic performance of the Pirajuba AUV. ANSYS Fluent was employed as a CFD solver by choosing the k-ω SST turbulence model for the simulation of the turbulent flow around AUV. According to the results, the control surface stall is determined by a linear relationship between the angle of attack and the control surface deflection. A majority of AUV simulations have been done using two-equation turbulence models, namely either k-ε or k–ω models.

Thanks to the swift advancement of contemporary computer technology, CFD has created a rush of interest in using high-fidelity computational techniques not just as an analysis tool but also as an optimization tool [2]. As a result, researchers have focused on the optimization of AUVs as a crucial aspect of improving their hydrodynamic efficiency and

reducing energy consumption [2]. AUV shape optimizations have been undertaken using different non-gradient optimization methods, such as Design of Experiment (DoE) [12] and stochastic optimization methods [13]. Joung et al. [12] optimized a torpedo-shaped AUV to minimize drag forces with consideration of three different design variables: the location of the sail relative to the bow, the separation between the sail and the acoustic, and the angle of attack of the nozzle. The turbulent flow around the AUV was simulated using the k-ε turbulence model in ANSYS-CFX. Besides, the optimal values of the design parameters were explored using the DOE method in ANSYS-Design Exploration. Alam et al. [13] developed an optimization framework based on a non-dominated sorting genetic algorithm (NSGA-II) and an infeasibility-driven evolutionary algorithm (IDEA) for single and multi-objective optimizations [13]. The framework was built by linking MATLAB and CATIA to reduce design cycle time. The framework was applied to optimize a hull AUV in terms of drag reduction. The optimized AUV was fabricated and tested in a swimming pool to measure the hydrodynamic forces. The experimental results were validated against CFD results obtained from ANSYS Fluent.

While the adjoint approach as a gradient-based method, has gained interest in shape optimization, particularly in turbomachinery, it has not been used for AUV optimization. The adjoint method provides an efficient way to compute derivatives of an objective function with respect to design variables with low computational cost independent of the number of design variables [14]. Therefore, this work aims to optimize an AUV using an adjoint solver available in OpenFOAM v2206 in terms of drag reduction. The second section outlines the numerical modelling, including governing equations, boundary conditions, mesh grid, AUV geometry, validation, and the optimization process. In the third section, the outcomes of AUV optimization are provided, and the article is then concluded.

2. Numerical modelling

A 3D steady-state Navier–Stokes incompressible solver (SimpleFoam) in OpenFOAM v2206 is employed to simulate the 3D turbulent flow around two AUV hulls. Besides, the AUV optimization has been carried out using a 3D steady-state adjoint Navier–Stokes incompressible solver (adjointOptimisationFoam) in OpenFOAM v2206.

2.1. Governing equations and numerical method

The governing equations are the Reynolds-averaged Navier-Stokes (RANS) equations for the steady flow of an incompressible fluid. The RANS equations are presented as follows:

$$R^P = \frac{-\partial v_j}{\partial x_j} = 0 \tag{1}$$

$$R_i^v = v_j \frac{\partial v_j}{\partial x_j} - \frac{\partial \tau_{ij}}{\partial x_j} + \frac{\partial p}{\partial x_i} = 0, i = 1, 2(, 3), \tag{2}$$

where $v_i$and p are the velocity components and the static pressure, respectively. Also, τ_{ij}= (ν +v_t) $\left(\frac{\partial v_i}{\partial x_j} + \frac{\partial v_j}{\partial x_i} \right)$represents the viscous stress tensor. ν and v_t denote the kinematic viscosity and turbulent viscosity, respectively. Yu et al. [15] and Hong et al. [16] found that the k-ω SST is more accurate than the k-ε RNG. Therefore, k-ω SST is used as a turbulence model. The adjoint equations should be derived using incompressible Navier-Stokes equations and the k-ω SST turbulence model. The derivation method is neglected here due to its extensive length. The final form of the adjoint mean-flow equations is proposed as follows:

$$R^q = \frac{-\partial u_j}{\partial x_j} = 0 \tag{3}$$

$$R_i^u = -v_j \frac{\partial u_j}{\partial x_j} + u_j \frac{\partial v_i}{\partial x_j} - \frac{\partial \tau_{ij}^a}{\partial x_j} + \frac{\partial q}{\partial x_i} + k_a \frac{\partial k}{\partial x_j} + \omega_a \frac{\partial k}{\partial x_j} + 2\frac{\partial}{\partial x_j}\left[\left(M_1 k_a v_t + \gamma \omega_a + M_3 \frac{C_{\Omega, v_t a_1 k}}{2\xi^3 F_2}\right)\left(\frac{\partial v_i}{\partial x_j} + \frac{\partial v_j}{\partial x_i}\right)\right. \quad (4)$$

where v_i, q, and τ_{ij}^adenote adjoint velocity components, the adjoint static pressure, and the adjoint viscous stress tensor. Also, several extra terms (denoted by M_l, l = 1, 2, 3).

To simulate the turbulent flow around the AUV, the two-equation turbulence model (k-ω SST) is used. For spatial discretization, a fully second-order method is applied to minimize excessive numerical dissipation while maintaining a predetermined degree of accuracy. The same approaches are also employed for solving the adjoint Navier-Stokes equations.

2.2. AUV geometry

The baseline AUV used in this study was designed by Alam et al. [13]. The AUV was globally optimized for drag reduction using two distinct gradient-free approaches (NSGA-II and IDEA) [13]. In this research, the AUV is locally optimized using the adjoint method. The AUV consists of three primary components: a nose cone, a parallel cylindrical mid-section, and a tapering tail section, as seen in Fig. 1.

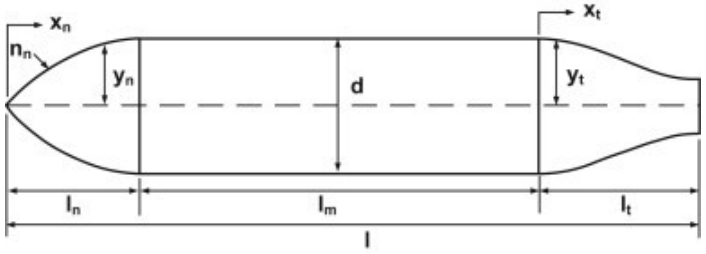

Fig. 1: The hull geometry parameterization [13].

The curvature of the nose and tail parts are obtained from Eqs. (5, 6):

$$y_n = \frac{1}{2} d + \left[1 - \left(\frac{l_n - x_n}{l_n}\right)^{n_n}\right]^{\frac{1}{n_n}} \quad (5)$$

where y_n, d, l_n, x_n, n_n, l_m represent the radius of the nose, the maximum body diameter, which may be changed, the length of the nose, the shape variation coefficient of the nose which may also be changed to create the different nose, and the mid-section length, respectively.

$$2\, y_t = 9.6556\, x_t^3 - 4.9\, x_t^2 + 0.05\, x_t + d \quad (6)$$

In Eq. (6), l_t, y_t, and x_t are the tail length, the tail radius, and the reference length, changed from 0 to l_t. The AUV created by SOLIDWORKS is shown in Fig. 2.

Fig. 2: The bare hull [13].

2.3. Boundary conditions & mesh grid

As the mid-section of AUV is cylindrical, the computational domain is also considered to be cylindrical to achieve a better mesh distribution over the entire domain. Fig. 3 depicts the computational domain. AUV with a length (L) of 1.3 m at distances of 17L from the inlet and outlet. Besides, the length of the domain and the diameter are 34L and 20L, respectively. A constant velocity (v = 2 m/s) with zero pressure gradient is imposed at the inlet (equivalent to a Reynolds number $Re_L = 2 \times 10^6$). No slip condition and zero pressure gradient are imposed on the AUV. Ambient pressure and zero velocity gradient are chosen for the outlet. Symmetry is imposed on the domain side.

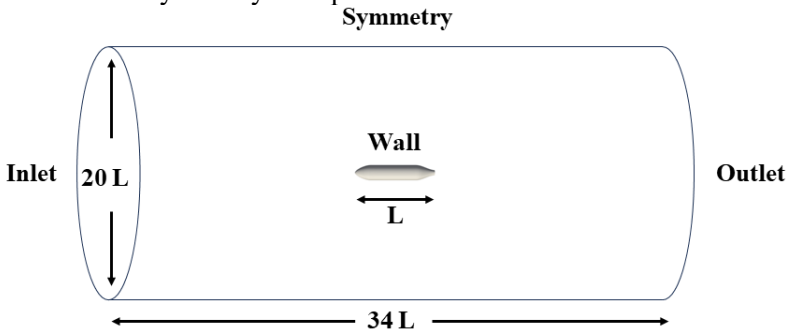

Fig. 3: Computational domain of AUV.

Salome is employed to generate an unstructured mesh grid for the computational domain, consisting of 26 prismatic layers around AUV. The computational domain has around two million mesh cells, including approximately 200,000 prismatic mesh cells and 1.8 million elements (Fig. 4). The maximum value of the wall coordinates y+ is around 0.9. Three distinct mesh grids (0.98 (coarse), 2.03 (medium), and 3.27 (fine) million cells) have been generated for the grid study. Approximately 3.3% and 0.15%, respectively, are the differences in drag force values between the coarse/medium and medium/fine meshes. Since the difference in drag force between medium and fine grids is negligible, the medium grid is used for all subsequent computations.

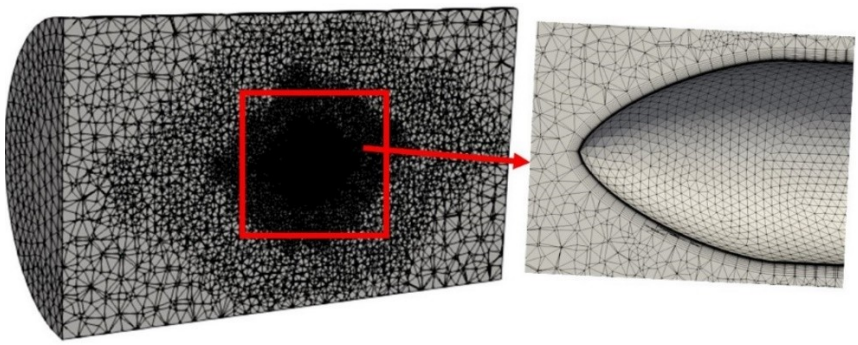

Fig. 4: The generated grid for the computational domain.

2.4. Validation

The drag force obtained from the present study is validated against numerical and experimental results by Alam et al. [13] and Saghafi and Lavimi [6]. As shown in Table 1, the drag force obtained in this study (medium mesh with 2 million) is 0.58% less than the experimental results.

Table 1: Comparison in terms of drag force for the baseline AUV between the present study and data from the literature.

	CFD solver	Turbulence model	Num. result (N)	Exp. result (N)
Alam et al. [13]	ANSYS Fluent	k-ε Realizable	9.448	9.6611
Saghafi and Lavimi [6]	ANSYS Fluent	k-ε Realizable	9.779	-
Present study	OpenFOAM v2206	k-ω SST	9.605	-

2.5. Optimization process

A 3D full continuous adjoint steady-state incompressible RANS solver (adjointOptimizationFoam) in OpenFOAM v2206 is used to optimize the nose and tail of AUV [17]. The continuous adjoint method was developed based on the k-ω SST turbulence model. To modify the nose and tail, a set of control points are generated around the nose and tail. The volume around the nose and tail of AUV hull is parameterized using volumetric Non-Uniform Rational B-Splines Modelling (NURBS), which are rational trivariate (in 3D) B-Splines defined on non-uniform knot vectors. During the optimization process, the constrained projection as an optimizer is employed as an optimizer to update the design variables by using the previously calculated sensitivity derivative.

In this study, drag force and partial volume are considered as objective function and constraint, respectively. Force (Eq. (22)) and partial volume (Eq. (23)) are defined as:

$$J_F = \frac{\int_{S_w} (p n_i - \tau_{ij n_j}) r_i \, d S_w}{\frac{1}{2} A U_\infty^2} \tag{7}$$

where S_w, n, r, A, and U_∞ represent the wall patches on which force is defined, the unit normal vector, the direction in which the force vector should be projected, the frontal area, and the far-field velocity magnitude, respectively.

$$J_V = \frac{V - V_{init}}{V_{init}} \tag{8}$$

where V and V_{init} are the volume enclosed by the patch defining S_w and the volume of the initial geometry, respectively.

3. Results and discussion

Fig. 5 depicts the variation of the objective function (drag force) with design cycles. Although the drag force reaches its lowest value during the first optimization cycle, the optimization process continues for two reasons. First, the optimization process is assumed to be converged if the objective function does not vary over subsequent optimization cycles. In this work, as there is no variation in the drag force from the ninth optimization, it is assumed that the optimization becomes converged. Second, the partial volume as a geometrical constraint should be constant. Yet, it varies over the early optimization cycles. The result indicates a 3.25% reduction in drag force after nine cycles. As seen in Fig. 6, the optimized nose exhibits a smoother curvature compared to the baseline. Besides, the optimized tail is slightly thicker than the baseline.

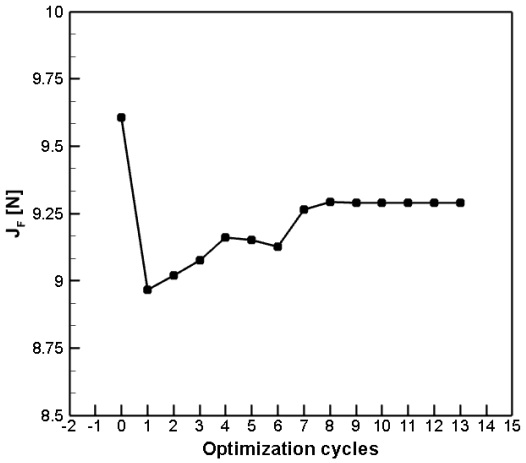

Fig. 5: History of the drag force.

Fig. 7 illustrates pressure coefficient contours around the baseline and optimized AUV. In the front of the nose, the region with the highest pressure is visible. This region is slightly diminished in optimized AUV. The magnitude velocity contours around the baseline and optimized AUVs are shown in Fig. 8. According to the velocity contours, the blue region around the tail, which has a zero speed, indicates the flow separation. As it can be seen, this region is weaker in the optimized AUV compared to the baseline.

(a) (b)

Fig. 6: Comparison of nose (a) and tail (b) between the baseline and optimized profiles.

4. Conclusion

This study focused on optimizing the nose and tail of an AUV using the adjoint technique. The drag force, which has a significant impact on energy consumption, was selected as an objective function to be reduced while the partial volume was considered as a constraint. The AUV length is 1.3 m which was optimized at a speed of 2 m/s ($Re_L = 2\times10^6$). Salome (CAD and mesh generator) and OpenFOAM v2206 (CFD solver and optimizer) were employed to perform the whole process. Reynolds-averaged Navier-Stokes equations with the k-omega SST turbulence model were used to simulate the turbulent flow around the AUV. The constrained AUV optimization was carried out using a 3D steady-state adjoint Navier-Stokes incompressible solver (adjointOptimisationFoam) in OpenFOAM v2206. A good agreement (a 0.58% disparity) was found when the drag force from study was validated against the experimental data. The results demonstrated that the optimized AUV achieved a 3.25% decrease in drag force compared to the baseline.

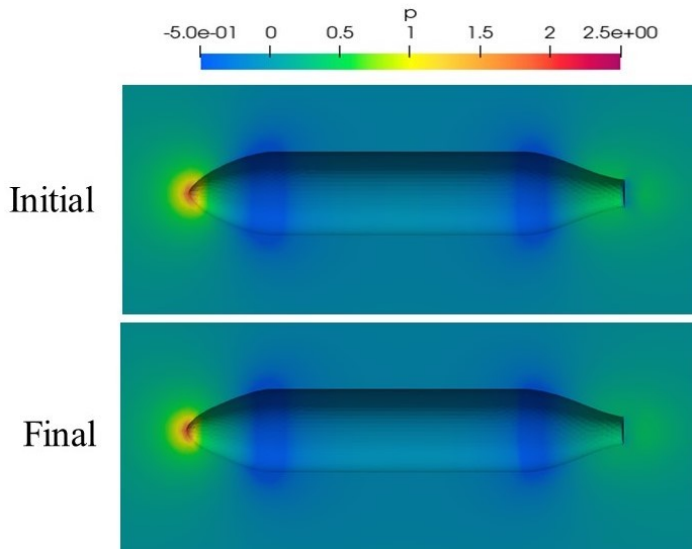

Fig. 7: Pressure contours of the baseline and optimized AUVs.

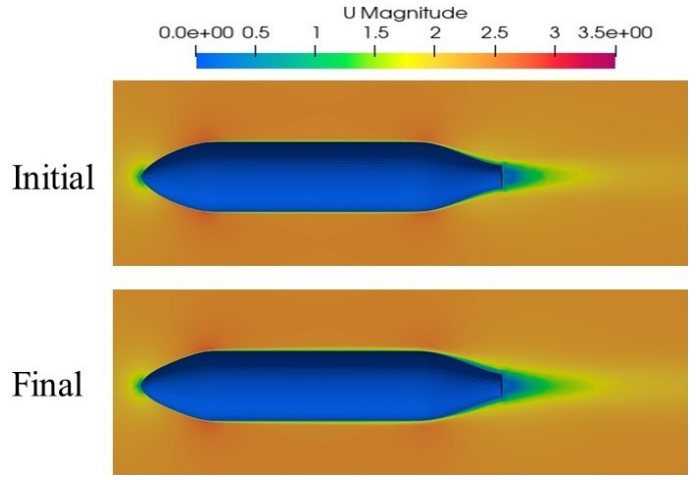

Fig. 8: Velocity magnitude contours around the baseline and optimized AUVs.

Acknowledgements

All computations were performed using the supercomputer Narval, managed by Scinet, and part of the Digital Research Alliance of Canada. The authors acknowledge also the financial support of NSERC through a CRD grant (No. RDCPJ 543679- 19).

References

[1] Sanchez, P. J. B., Papaelias, M., and Marquez, F. P. G., 2020. “Autonomous underwater vehicles: Instrumentation and measurements”. IEEE Instrumentation & Measurement Magazine, 23(2), pp. 105–114.

[2] Chen, X., Yu, L., Liu, L. Y., Yang, L., Xu, S., and Wu, J., 2023. “Multi-objective shape optimization of autonomous underwater vehicle by coupling CFD simulation with genetic algorithm”. Ocean Engineering, 286, 115722.

[3] Roper, D. T., Phillips, A. B., Harris, C. A., Salavasidis, G., Pebody, M., Templeton, R., Amma, S. V. S., Smart, M., and McPhail, S., 2017. “Autosub long range 1500: An ultraendurance AUV with 6000 km range”. In OCEANS 2017-IEEE Aberdeen, Scotland, pp. 1–5.
[4] Raman, N., Briscoe, J. D., and Grivel, T., 2002. “Lithium-ion batteries for autonomous underwater vehicles”. In Proceedings of the 2002 Workshop on Autonomous Underwater Vehicles, IEEE, San Antonio, USA, pp. 45–49.
[5] d’Amore Domenech, R., Raso, M. A., Villalba-Herreros, A., Santiago, O., Navarro, E., and Leo, T. J., 2018. “Autonomous underwater vehicles powered by fuel cells: Design guidelines”. Ocean Engineering, 153, pp. 387–398.
[6] Saghafi, M., and Lavimi, R., 2020. “Optimal design of nose and tail of an autonomous underwater vehicle hull to reduce drag force using numerical simulation”. Proceedings of the Institution of Mechanical Engineers, Part M: Journal of Engineering for the Maritime Environment, 234(1), pp. 76–88.
[7] Panda, J. P., Mitra, A., and Warrior, H. V., 2021. “A review on the hydrodynamic characteristics of autonomous underwater vehicles”. Proceedings of the Institution of Mechanical Engineers, Part M: Journal of Engineering for the Maritime Environment, 235(1), pp. 15–29.
[8] Madan, A., and Issac, M. T., 2017. “Hydrodynamic analysis of AUV hulls using semi-empirical and CFD approach”. Universal Journal of Mechanical Engineering, 5(5), pp. 137–143.
[9] Saeidinezhad, A., Dehghan, A. A., and Manshadi, M. D., 2015. “Experimental investigation of hydrodynamic characteristics of a submersible vehicle model with a nonaxisymmetric nose in pitch maneuver”. Ocean Engineering, 100, pp. 26–34.
[10] Dantas, J. L. D., and De Barros, E., 2013. “Numerical analysis of control surface effects on AUV manoeuvrability”. Applied Ocean Research, 42, pp. 168–181.
[11] Liu, X., Yuan, Q., Zhao, M., Cui, W., and Ge, T., 2017. “Multiple objective multidisciplinary design optimization of heavier-than-water underwater vehicle using CFD and approximation model”. Journal of Marine Science and Technology, 22, pp. 135–148.
[12] Joung, T.-H., Sammut, K., He, F., and Lee, S.-K., 2012. “Shape optimization of an autonomous underwater vehicle with a ducted propeller using computational fluid dynamics analysis”. International Journal of Naval Architecture and Ocean Engineering, 4(1), pp. 44–56.
[13] Alam, K., Ray, T., and Anavatti, S. G., 2014. “Design and construction of an autonomous underwater vehicle”. Neurocomputing, 142, pp. 16–29.
[14] Wang, D., and He, L., 2010. “Adjoint aerodynamic design optimization for blades in multistage turbomachines—part I: Methodology and verification”. Journal of Turbomachinery, 132(2), 021011.
[15] Yu, X., Su, Y., Wang, Z., and Yang, L., 2008. “Numerical simulation of drag on mini underwater vehicle”. In Symposium on Naval Hydrodynamics, Hangzhou, China, pp. 128–132.
[16] Hong, L., Fang, R., Cai, X., and Wang, X., 2021. “Numerical investigation on hydrodynamic performance of a portable AUV”. Journal of Marine Science and Engineering, 9(8), p. 812.
[17] Giannakoglou, K., Papoutsis-Kiachagias, E., and Gkaragkounis, K., 2020. adjointOptimisationFoam, an OpenFOAM-based Optimization Tool. Parallel CFD & Optimisation Unit, School of Mechanical Engineering, National Technical University of Athens, Greece